Article

Reversing the Activity Center in Doped $Pd_{17}Se_{15}$ to Achieve High Stability Toward the Electrochemical Hydrogen Evolution Reaction

Saurav Ch. Sarma, Sai Manoj Kaja, K. A. Ann Mary, and Sebastian C. Peter*

Cite This: *ACS Appl. Energy Mater.* 2020, 3, 4051−4056

Read Online

ACCESS | 📊 Metrics & More | 📰 Article Recommendations | 🆂🅸 Supporting Information

ABSTRACT: The use of hydrogen, being an environmentally cleaner source of energy, may reduce the pressing problem of CO_2 emissions due to the burning of conventional fossil fuels. However, the prolonged production of hydrogen is a major issue and can be solved through designing a stable electrocatalyst. In this work, we have designed a Ni-doped $Pd_{17}Se_{15}$ catalyst that retains its activity for 20000 electrochemical cycles. The enhanced stability of this electrocatalyst can be attributed to the reversal of the activity center from the Pd to the Se center through Ni substitution. The concept of activating the chalcogen center and deactivating the Pd site is supported through theoretical calculations. This work provides a unique strategy of tuning catalysts toward higher activity and stability.
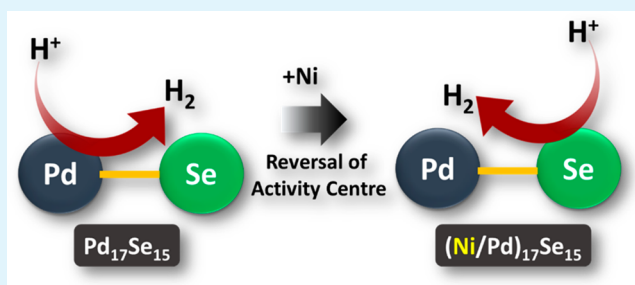
■ INTRODUCTION

Environmental pollution and global warming are two major concerns of the past few decades. Resorting to an alternative source of energy can prove to be a better choice for sustainable development. The hydrogen economy has the potential for mitigating the problem of global warming through the reduction of greenhouse gases.[1] However, generating an inexpensive source of hydrogen is still a challenge. The hydrogen evolution reaction (HER) is a photo/electrochemical process in which water is reduced to molecular hydrogen. With increasing emphasis recently placed on sustainable energy harvesting and conversion, this particular reaction has gained mounting attention for its pivotal role in electrolytic or photocatalytic water splitting.

Generating a significant amount of hydrogen for a prolonged period is still a challenge through electrochemical splitting mainly due to poor stability of the electrocatalyst in an electrolyte medium. First, the strong adsorption of the anionic intermediates (SO_4^{2-}, ClO_4^{2-}) on the catalyst surface can accelerate the degradation over time. Second, the stronger hydrogen adsorption enables faster proton supply for the reaction, leading to weaker hydrogen desorption and slower release of active sites, thus poisoning the catalyst surface. Hydrogen adsorption that is too weak will lead to inefficient proton supply, resulting in a sluggish HER rate. Therefore, it is crucial to control the behavior of H_2 adsorption so that the adsorption is neither strong nor too weak.

Both of these associated issues can be resolved by changing the active center from the most vulnerable metallic site to the less vulnerable nonmetallic site. From a fundamental perspective, the transfer of activity from the metal to nonmetal site provides us with two advantages: (i) the reduced activity of the metallic site and enhanced activity of the nonmetallic site can demonstrate enhanced stability during a reaction due to reduced poisoning by the anionic and neutral adsorbate, and (ii) since the metal site contributes negligibly to the overall activity, lowering the loading percentage of the noble metal is barely expected to affect the activity of the catalyst.

However, the precise tuning of the electronic structure is required to achieve such an idea of reversing the activity. Previous literature has proven that alloying techniques can show genuine potential to obtain the required electronic structure that is substantially different from the constituent element.[2−11] Alloying can induce an electronic structure change into the system due to strain (strain/geometric effect)[12,13] and due to the introduction of a secondary element (ligand effect).[14−18]

Recently, some chalcogenide materials have been reported to exhibit a high degree of hydrogen evolution activity.[19−27] Most of them have reported chalcogen surface sites as the active center toward hydrogen adsorption.[28] ZrS_2, $ZrSe_2$, and ZrSSe are theoretically predicted to have better HER activity.[29] They show more activity in the chalcogenide center. The
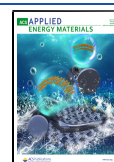
electronic structure of such binary chalcogenides can further be tuned by the introduction of a secondary element into the lattice.

Motivated by our previous works on $CoPd_2Se_2$,[30] $Pd_{17}Se_{15}$,[31] and $(Cu/Pd)_{17}Se_{15}$,[4] which demonstrated better activity and stability through alloying/substitution, we performed electrochemical studies on $(Ni/Pd)_{17}Se_{15}$ to generalize the high stability of Pd-based chalcogenides. We believe that the asymmetric distribution of electron density on such chalcogenide systems generates an adsorption site that favors the coupling of two *H to form a H–H bond.

■ RESULTS AND DISCUSSION

In the following sections, we discussed the following three scientific points:

(1) The effect of the electronic structure on the oxidation state, electronic structure, and charge distribution on the catalyst surface.

(2) The driving force for enhancement of the activity.

(3) The reason for the higher stability of the electrocatalyst.

We synthesized $Pd_{17}Se_{15}$ and were able to achieve a reversal of activity by tuning Pd to be more electropositive and Se to be more electronegative. Pd in its 2+ state has a weaker adsorption toward hydrogen and hence becomes deactivated for the HER. Because of its 2− state, Se has extra electron density near the Fermi level and hence becomes active for HER.[4,31] Alloying with Ni further tunes the electronic structure of the catalyst to have optimized adsorption of H on the chalcogen site.

The catalysts were synthesized by the colloidal method using $Ni(acac)_2$, $Pd(acac)_2$, and selenous acid as the precursors at a stoichiometric ratio of 1:2:2, respectively. The temperature was fixed at 220 °C for 3 h. To understand the nature of the doped $Pd_{17}Se_{15}$, we carried out characterization using scanning electron microscopy (SEM), transmission electron microscopy (TEM), X-ray diffraction (XRD), EDAX, and X-ray absorption spectroscopy (XAS).

In order to reflect the inverse strain behavior, as we proposed in our previous work, we collected powder XRD (PXRD) at a very slow scan rate for a longer duration of time, as shown in Figures 1 and S1. We emphasize here an expected shift of the PXRD peak position toward a higher 2θ. However, this observation is contrary to the trend observed in $(CuPd)_{17}Se_{15}$. A shift toward a higher 2θ is representative of a decrease in the unit cell size of the substituted compound.

Figures 1b and 1c show the aggregated nature of the nanoparticles due to the $NaBH_4$ reduction method used during the synthesis process. This method results in the formation of small-sized nanoparticles of higher surface area due to the presence of dangling bonds. Such small-sized particles tend to agglomerate to reduce their high surface energy and hence form connected nanostructures.[32,33] Such particles also confirm the polycrystalline nature, as evidenced from the selected area electron diffraction (SAED) pattern shown in Figure 1d. As per the EDAX analysis, the atomic percentages of Ni, Pd, and Se are ~8.8, ~35.5, and ~55.7%, respectively. To understand the oxidation state on Se, XANES spectroscopy was recorded at a synchrotron facility at RRCAT Indore, India, as shown in Figure S2. Se foil and CoSe/NiSe with a zero and −2 oxidation state were used as the references for understanding the relative oxidation state on $(Ni/Pd)_{17}Se_{15}$. Both $(Cu/Pd)_{17}Se_{15}$ and $(Ni/Pd)_{17}Se_{15}$ have been found to have
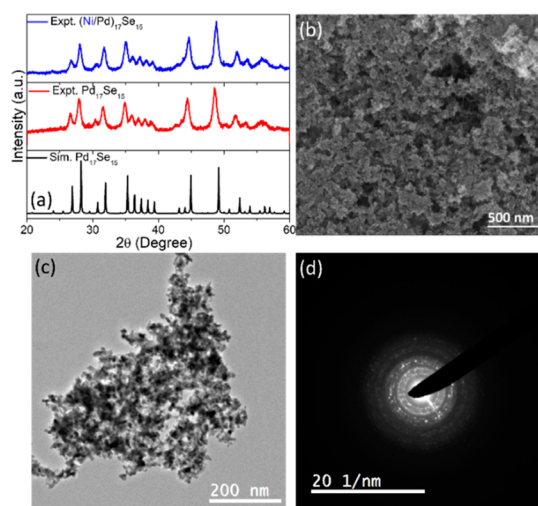

Figure 1. (a) PXRD pattern of substituted $(Ni/Pd)_{17}Se_{15}$, (b) morphology as obtained from SEM images, (c) TEM images, and (d) selected area electron diffusion (SAED) pattern of $(Ni/Pd)_{17}Se_{15}$.

closer to a −2 oxidation state in comparison to the near zero oxidation state on $Pd_{17}Se_{15}$, indicating similar behavior upon the substitution of Cu or Ni in the $Pd_{17}Se_{15}$ lattice.

Electrochemical Activity and Stability. Electrochemical activation of the catalyst was performed for 100 cycles in nitrogen-purged 0.5 M H_2SO_4 with a scan rate of 50 mV/s. The catalyst exhibited better onset after the activation process, as shown in Figure S3a, which may be attributed to the surface rearrangement or dissolution of Ni from the catalyst. Apparently, the onset potential and the overpotential at 10 mA/cm^2 are frequently used to directly evaluate the HER. The onset overpotential is defined as the overpotential (vs RHE) of the current density at 1 mA/cm^2. The catalyst exhibited an onset potential of 92 mV, and a current density of 10 mA/cm^2 was obtained at an overpotential of 197 mV (Figure 2a). An accelerated degradation test (ADT) was performed at a higher scan rate of 100 mV/s, and a negligible shift was observed after 20000 electrochemical cycles. This indicates the better stability of the catalyst, which is due to the reversal of the activity center, as described in the subsequent section. Electrochemical impedance data were collected at a regular interval to keep track of the charge-transfer resistance (R_{ct}) during the ADT. A smaller R_{ct} of ~75 Ω was obtained at the end of the ADT (Figure 2b).

The electrochemical surface area of a catalyst is in general directly correlated to the catalyst activity, and it was evaluated for our samples using cyclic voltammetry (CV) to obtain double-layer capacitive currents (Figures 2c and S3). The double-layer capacitance was calculated by fitting the linear plot of the capacitive current versus the scan rate. A change in the C_{dl} of the catalyst from 1.30 to 1.21 mF/cm^2 was observed after the stability test with 20000 electrochemical cycles. Thus, no significant surface area change was observed during the course of ADT. A chronoamperometry test was performed for 24 h at an overpotential of 200 mV. No significant decrease in the current density was observed at the end of 24 h, indicating the high stability of the catalyst (Figure 2d). The overlapping polarization curve after the CA test also corroborates with the better stability of the catalyst (Figure S4). To understand the reaction mechanism, the Tafel slope was extracted by plotting log j versus the overpotential and fitting its linear portion at a
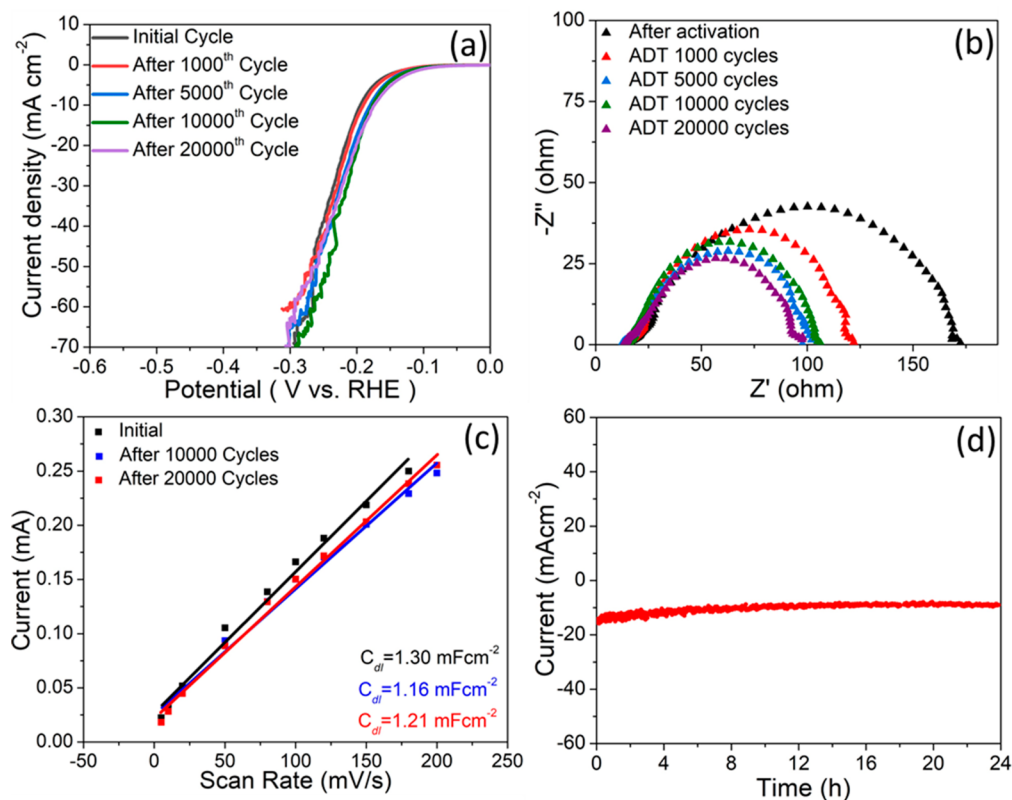
Figure 2. (a) HER polarization plots of $(Ni/Pd)_{17}Se_{15}$ surface in 0.5 M H_2SO_4 as a function of cycling number. (b) Variation of the electrochemical impedance data for the sample with cycle number. (c) Linear fitting of the capacitive currents of samples in 0.5 M H_2SO_4 vs scan rates. (d) Time dependence of current density of $(Ni/Pd)_{17}Se_{15}$ in 0.5 M H_2SO_4 under a static overpotential of 0.2 V vs RHE.

Figure 3. (a) Bonding information in the crystal. 2D electron localization function mapping of the (100) surface of Pd, NiA, NiB, and NiC with an isosurface value of 0.8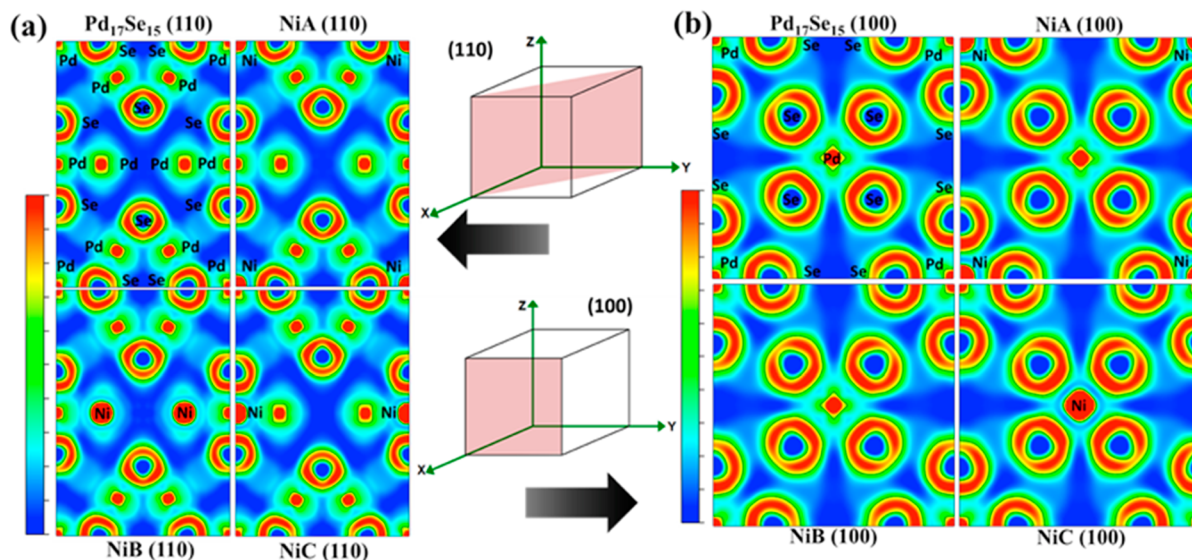. (b) Bonding information in the crystal. 2D electron localization function mapping of the (110) surface of Pd, NiA, NiB, and NiC with an isosurface value of 0.8.

low overpotential. A Tafel slope of 91.5 mV/dec was extracted from the polarization curve and reported in Figure S5. As shown previously,[34,35] a Tafel slope close to ~120 mV/dec indicates the Volmer adsorption process as the rate-determining step. Figure S5 shows the change in the Tafel slope value after CA and ADT tests. The robust catalytic performance mainly arose from the less vulnerable chalcogenide site.

Theoretical Calculation. In order to gain insight into the change of the electronic structure and charge distribution upon Ni substitution, we performed DFT calculations. Three input models were designed, namely NiA, NiB, and NiC, with three different sites of Ni substitution, as shown in Figure S6. Energy-optimized $Pd_{17}Se_{15}$, NiA, NiB, and NiC have a lattice parameter of 10.7403, 10.7228, 10.6358, and 10.6944 Å, respectively. A decrease in the cell parameter of the unit cell is
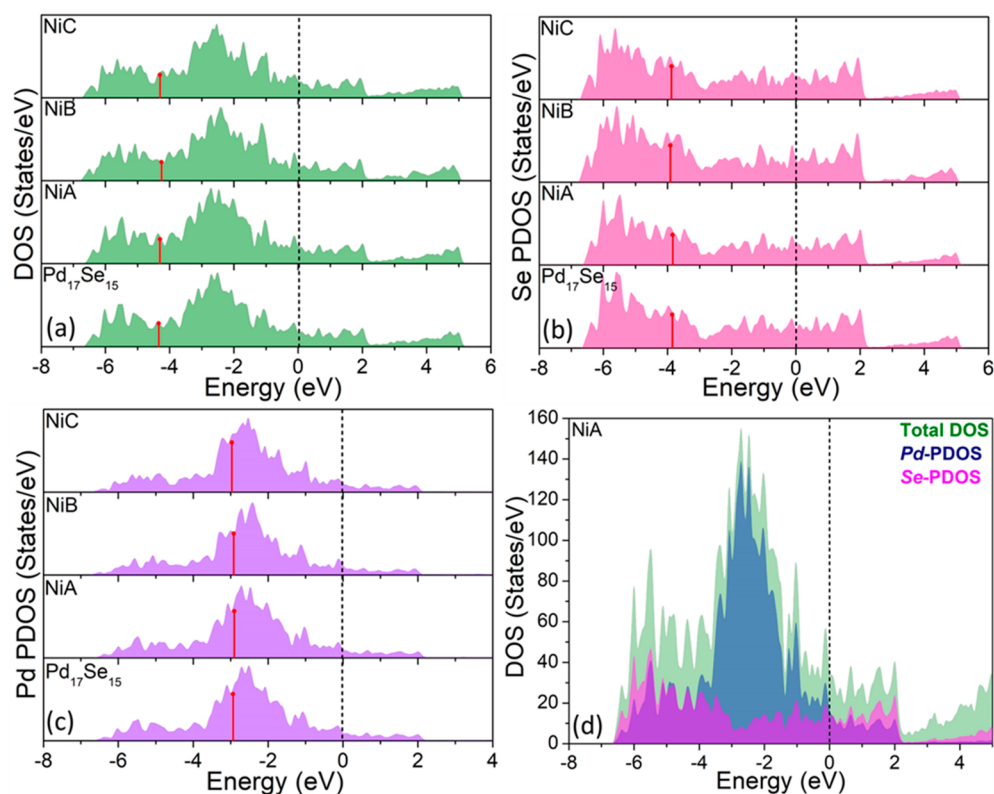
Figure 4. (a) DOS, (b) Se-PDOS, and (c) Pd-PDOS of $Pd_{17}Se_{15}$, NiA, NiB, and NiC. (d) The combination of Pd-PDOS, Se-PDOS, and total DOS shows that the Fermi level has a dominant contribution from both Pd and Se.

clearly reflected by the shift in the PXRD peak position toward a higher 2θ. Because the radius of the Ni atom is smaller than that of the Pd atom, Ni doping produces strain in the lattice. The ligand effect caused by Ni doping in $Pd_{17}Se_{15}$ also has the potential to affect H adsorption and desorption through modification of the electronic structure. This subtle modification in the d-band electronic structure, caused by both the strain and ligand effect, may result in an amplified change in the electrocatalytic activity and stability.[36] The change in the electronic structure is clearly reflected by probing the charge distribution and density of states of an electrocatalyst.

In order to understand the effect on the electronic structure upon Ni substitution, we performed cell (energy + lattice parameter) optimization. A 2D electron localization function (ELF) is then plotted for a few planes to observe the change in the electron distribution. ELF yields the probability of finding an electron near another electron with the opposite spin, which is typical for chemical bonds and electron lone pairs.[37] It is a measure of localized electron density which can differentiate between different types of bonding, e.g., metallic, ionic, or covalent. The maximum ELF value of 1 denotes complete electron localization (shown as red regions in Figures 3), whereas an ELF value of 0.5 corresponds to a delocalized ideal electron gas (green). Most of the space between atoms is blue (ELF $\approx$ 0), indicating a localized electron cloud consistent with polar covalent bonding. This additional ionic contribution could explain the added stability of the compound over purely metallic bonding in Pd.[38] A high ELF value is colored red, and the series descends through yellow, green, turquoise, and blue. The localized charge distribution is different for NiA (100) and NiC (100) in Figure 3a; NiA (110), NiB (110), and NiC (110) in Figure 3b; and NiC (111) in Figure S7, which

demonstrates the change in ELF due to substitution by Ni. There was no Ni substituted in the (100) plane of NiB, and hence, it completely replicated the ELF of pristine $Pd_{17}Se_{15}$. Figure 3a and 3b show that there is a polar covalent interaction between the atoms. An increase in the electron density is observed upon Ni substitution. This is represented by the increase in the size of the red-colored density on Ni. This signifies that Ni and Se interact strongly due to the greater electron delocalization over the Ni−Se bond compared to the Pd−Se bond.

In order to understand the role of Pd or Se in the activity of the catalyst, the PDOS of Pd d and Se p states are plotted along with their d-band centers. The shift of the d-band center toward the Fermi level (Figures 4a and S8) strengthens the adsorbate bonding. The distribution of the electron density over the Ni−Se bond is clearly reflected by the shift of the d-band center toward the Fermi level (Figure 4b), thus strengthening the nonmetal−adsorbate bonding. This further activates the Se sites for electrochemical HER by lowering the ΔG_{ads} to a value near 0. A similar shift toward the Fermi level is observed for the Pd d-band center, as shown in Figure 4c. However, such a shift further lowers the ΔG_{ads} to have a more negative value and hence deactivates it for HER. This clearly explains the reversal of activity from the metal to nonmetal center. A considerable contribution to the local density of states (DOS) near the Fermi level could act as electron donors for the adsorbed molecules. Thus, clear participation of Se in the electrochemical HER was observed due to the significant contribution of Se PDOS near the Fermi level (Figure 4d).[39] The orbital analysis showed that the surface states mainly comprise p-like electronic states from the Se.

To evaluate the effect of the strain, we built a model with the same strain as $(Ni/Pd)_{17}Se_{15}$ but without Ni substitution by fixing the bond length of $(Ni/Pd)_{17}Se_{15}$. Similarly, the ligand effect was deconvoluted by constraining $(Ni/Pd)_{17}Se_{15}$ to have a lattice parameter of $Pd_{17}Se_{15}$. Thus, now we have a ligand incorporated into the lattice without any change in the lattice parameter. This gives us the deconvoluted ligand and strain effect. The effect on the DOS was recorded as a descriptor for this deconvolution. The calculation results show that both the compressive strain and ligand effects contribute to the enhanced activity (Figure 5).
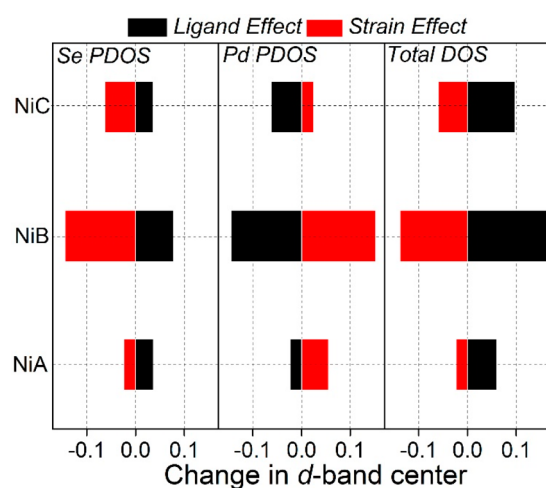

Figure 5. Deconvolution of strain and ligand effect on Se and Pd sites of $(Ni/Pd)_{17}Se_{15}$.

However, it can clearly be noticed that the trend of strain and ligand effect for Pd is reversed compared to that in Se and the total DOS. Thus, the contribution from Se to the total DOS is appreciable compared to Pd.

CONCLUSION

In conclusion, we have synthesized a $(Ni/Pd)_{17}Se_{15}$ catalyst that is stable for 20000 electrochemical cycles during a hydrogen evolution reaction. The reversal of the active center from Pd to Se is responsible for the higher stability of the electrocatalyst. Se, due to its anionic nature, is highly resistant toward the anionic intermediate. Furthermore, H adsorption is optimal due to the tuning by Ni substitution. This concept of the reversal of the activity center can be exploited to design a catalyst with better stability, which is a major concern for the prolonged production of hydrogen through electrochemical water splitting.

ASSOCIATED CONTENT

Ⓢ Supporting Information

The Supporting Information is available free of charge at https://pubs.acs.org/doi/10.1021/acsaem.0c00512.

Experimental details, electrochemical studies, theoretical calculation, crystal structure, PXRD, XANES, LSV, CV polarization curve, Tafel slope, ELF, and DOS (PDF)

AUTHOR INFORMATION

Corresponding Author

Sebastian C. Peter − New Chemistry Unit and School of Advanced Materials, Jawaharlal Nehru Centre for Advanced Scientific Research Jakkur, Bengaluru 560064, Karnataka, India; ● orcid.org/0000-0002-5211-446X; Email: sebastiancp@jncasr.ac.in

Authors

Saurav Ch. Sarma − New Chemistry Unit and School of Advanced Materials, Jawaharlal Nehru Centre for Advanced Scientific Research Jakkur, Bengaluru 560064, Karnataka, India; ● orcid.org/0000-0002-6941-9702

Sai Manoj Kaja − New Chemistry Unit and School of Advanced Materials, Jawaharlal Nehru Centre for Advanced Scientific Research Jakkur, Bengaluru 560064, Karnataka, India

K. A. Ann Mary − Department of Physics, St. Thomas College, Thrissur 680001, Kerala, India

Complete contact information is available at:
https://pubs.acs.org/10.1021/acsaem.0c00512

Notes

The authors declare no competing financial interest.

REFERENCES

(1) Ren, J.; Gao, S.; Liang, H.; Tan, S.; Dong, L. The Role of Hydrogen Energy: Strengths, Weaknesses, Opportunities, and Threats. In *Hydrogen Economy*; Scipioni, A., Manzardo, A., Ren, J., Eds. Academic Press: 2017; pp 1−33.

(2) Gasteiger, H. A.; Kocha, S. S.; Sompalli, B.; Wagner, F. T. Activity benchmarks and requirements for Pt, Pt-alloy, and non-Pt oxygen reduction catalysts for PEMFCs. *Appl. Catal., B* **2005**, *56* (1), 9−35.

(3) Bing, Y.; Liu, H.; Zhang, L.; Ghosh, D.; Zhang, J. Nano-structured Pt-alloy electrocatalysts for PEM fuel cell oxygen reduction reaction. *Chem. Soc. Rev.* **2010**, *39* (6), 2184−2202.

(4) Sarma, S. C.; Mishra, V.; Ann Mary, K. A.; Roy, S.; Peter, S. C. Inverse Strain Effect in Atomic Scale"—Enhanced Hydrogen Evolution Activity and Durability in Cu-Substituted Palladseite. *ACS Energy Lett.* **2018**, *3* (12), 3008−3014.

(5) Lang, X.-Y.; Han, G.-F.; Xiao, B.-B.; Gu, L.; Yang, Z.-Z.; Wen, Z.; Zhu, Y.-F.; Zhao, M.; Li, J.-C.; Jiang, Q. Mesostructured Intermetallic Compounds of Platinum and Non-Transition Metals for Enhanced Electrocatalysis of Oxygen Reduction Reaction. *Adv. Funct. Mater.* **2015**, *25* (2), 230−237.

(6) Sarma, S. C.; Subbarao, U.; Khulbe, Y.; Jana, R.; Peter, S. C. Are we underrating rare earths as an electrocatalyst? The effect of their substitution in palladium nanoparticles enhances the activity towards ethanol oxidation reaction. *J. Mater. Chem. A* **2017**, *5* (44), 23369−23381.

(7) Sarma, S. C.; Peter, S. C. Understanding small-molecule electro-oxidation on palladium based compounds - a feature on experimental and theoretical approaches. *Dalton Transactions* **2018**, *47* (24), 7864−7869.

(8) Jana, R.; Dhiman, S.; Peter, S. C. Facile solvothermal synthesis of highly active and robust $Pd_{1.87}Cu_{0.11}Sn$ electrocatalyst towards direct ethanol fuel cell applications. *Mater. Res. Express* **2016**, *3* (8), 084001.

(9) Jana, R.; Subbarao, U.; Peter, S. C. Ultrafast synthesis of flower-like ordered Pd_3Pb nanocrystals with superior electrocatalytic activities towards oxidation of formic acid and ethanol. *J. Power Sources* **2016**, *301*, 160−169.

(10) Sarkar, S.; Jana, R.; Suchitra; Waghmare, U. V.; Kuppan, B.; Sampath, S.; Peter, S. C. Ordered Pd_2Ge Intermetallic Nanoparticles as Highly Efficient and Robust Catalyst for Ethanol Oxidation. *Chem. Mater.* **2015**, *27* (21), 7459−7467.

(11) Sarkar, S.; Peter, S. C. An Overview on Pd Based Electrocatalysts for Hydrogen Evolution Reaction. *Inorg. Chem. Front.* **2018**, *5*, 2060−2080.

(12) Mavrikakis, M.; Hammer, A. B.; Nørskov, J. K. Effect of Strain on the Reactivity of Metal Surfaces. *Phys. Rev. Lett.* **1998**, *81* (13), 2819−2822.

(13) Rajamani, A. R.; Ashly, P. C.; Dheer, L.; Sarma, S. C.; Sarkar, S.; Bagchi, D.; Waghmare, U. V.; Peter, S. C. Synergetic Effect of Ni-Substituted Pd_2Ge Ordered Intermetallic Nanocomposites for Efficient Electrooxidation of Ethanol in Alkaline Media. *ACS Appl. Energy Mater.* **2019**, *2* (10), 7132−7141.

(14) Hammer, B.; Nørskov, J. K. Theoretical surface science and catalysis—calculations and concepts. In *Adv. Catal.*; Academic Press: 2000; Vol. *45*, pp 71−129.

(15) Stamenkovic, V.; Mun, B. S.; Mayrhofer, K. J. J.; Ross, P. N.; Markovic, N. M.; Rossmeisl, J.; Greeley, J.; Nørskov, J. K. Changing the Activity of Electrocatalysts for Oxygen Reduction by Tuning the Surface Electronic Structure. *Angew. Chem.* **2006**, *118* (18), 2963−2967.

(16) Jana, R.; Bhim, A.; Bothra, P.; Pati, S. K.; Peter, S. C. Electrochemical Dealloying of $PdCu_3$ Nanoparticles to Achieve Pt-like Activity for the Hydrogen Evolution Reaction. *ChemSusChem* **2016**, *9* (20), 2922−2927.

(17) Sarkar, S.; Dheer, L.; Vinod, C. P.; Thapa, R.; Waghmare, U. V.; Peter, S. C. Stress-Induced Electronic Structure Modulation of Manganese-Incorporated Ni_2P Leading to Enhanced Activity for Water Splitting. *ACS Appl. Energy Mater.* **2020**, *3* (2), 1271−1278.

(18) Sarkar, S.; Subbarao, U.; Peter, S. C. Evolution of dealloyed $PdBi_2$ nanoparticles as electrocatalysts with enhanced activity and remarkable durability in hydrogen evolution reactions. *J. Mater. Chem. A* **2017**, *5* (30), 15950−15960.

(19) McAllister, J.; Bandeira, N. A. G.; McGlynn, J. C.; Ganin, A. Y.; Song, Y.-F.; Bo, C.; Miras, H. N. Tuning and mechanistic insights of metal chalcogenide molecular catalysts for the hydrogen-evolution reaction. *Nat. Commun.* **2019**, *10* (1), 370.

(20) Tiwari, A. P.; Kim, D.; Kim, Y.; Prakash, O.; Lee, H. Highly active and stable layered ternary transition metal chalcogenide for hydrogen evolution reaction. *Nano Energy* **2016**, *28*, 366−372.

(21) De Silva, U.; Masud, J.; Zhang, N.; Hong, Y.; Liyanage, W. P. R.; Asle Zaeem, M.; Nath, M. Nickel telluride as a bifunctional electrocatalyst for efficient water splitting in alkaline medium. *J. Mater. Chem. A* **2018**, *6* (17), 7608−7622.

(22) Damien, D.; Anil, A.; Chatterjee, D.; Shaijumon, M. M. Direct deposition of $MoSe_2$ nanocrystals onto conducting substrates: towards ultra-efficient electrocatalysts for hydrogen evolution. *J. Mater. Chem. A* **2017**, *5* (26), 13364−13372.

(23) Chia, X.; Ambrosi, A.; Lazar, P.; Sofer, Z.; Pumera, M. Electrocatalysis of layered Group 5 metallic transition metal dichalcogenides (MX_2, M = V, Nb, and Ta; X = S, Se, and Te). *J. Mater. Chem. A* **2016**, *4* (37), 14241−14253.

(24) Wei, C.; Wu, W.; Li, H.; Lin, X.; Wu, T.; Zhang, Y.; Xu, Q.; Zhang, L.; Zhu, Y.; Yang, X.; Liu, Z.; Xu, Q. Atomic Plane-Vacancy Engineering of Transition-Metal Dichalcogenides with Enhanced Hydrogen Evolution Capability. *ACS Appl. Mater. Interfaces* **2019**, *11* (28), 25264−25270.

(25) Pan, Z.-H.; Tao, Y.-W.; He, Q.-F.; Wu, Q.-Y.; Cheng, L.-P.; Wei, Z.-H.; Wu, J.-H.; Lin, J.-Q.; Sun, D.; Zhang, Q.-C.; Tian, D.; Luo, G.-G. The Difference Se Makes: A Bio-Inspired Dppf-Supported

(26) Huang, D.-D.; Li, S.; Wu, Y.-P.; Wei, J.-H.; Yi, J.-W.; Ma, H.-M.; Zhang, Q.-C.; Liu, Y.-L.; Li, D.-S. In situ synthesis of a Fe_3S_4/MIL-53(Fe) hybrid catalyst for an efficient electrocatalytic hydrogen evolution reaction. *Chem. Commun.* **2019**, *55* (31), 4570−4573.

(27) Luo, G.-G.; Zhang, H.-L.; Tao, Y.-W.; Wu, Q.-Y.; Tian, D.; Zhang, Q. Recent progress in ligand-centered homogeneous electrocatalysts for hydrogen evolution reaction. *Inorg. Chem. Front.* **2019**, *6* (2), 343−354.

(28) Yang, X.; Zhao, Z.; Yu, X.; Feng, L. Electrochemical hydrogen evolution reaction boosted by constructing Ru nanoparticles assembled as a shell over semimetal Te nanorod surfaces in acid electrolyte. *Chem. Commun.* **2019**, *55* (10), 1490−1493.

(29) Som, N. N.; Jha, P. K. Hydrogen evolution reaction of metal dichalcogenides: ZrS_2, $ZrSe_2$ and Janus ZrSSe. *Int. J. Hydrogen Energy* **2019** .

(30) Sarma, S. C.; Mishra, V.; Vemuri, V.; Peter, S. C. Breaking the O═O Bond": Deciphering the Role of Each Element in Highly Durable $CoPd_2Se_2$ toward Oxygen Reduction Reaction. *ACS Appl. Energy Mater.* **2020**, *3* (1), 231−239.

(31) Sarma, S. C.; Vemuri, V.; Mishra, V.; Peter, S. C. Sacrificial protection in action!": ultra-high stability of palladseite mineral towards the oxygen reduction reaction. *J. Mater. Chem. A* **2019**, *7* (3), 979−984.

(32) Fu, S.; Zhu, C.; Du, D.; Lin, Y. Facile One-Step Synthesis of Three-Dimensional Pd-Ag Bimetallic Alloy Networks and Their Electrocatalytic Activity toward Ethanol Oxidation. *ACS Appl. Mater. Interfaces* **2015**, *7* (25), 13842−13848.

(33) Du, W.; Mackenzie, K. E.; Milano, D. F.; Deskins, N. A.; Su, D.; Teng, X. Palladium-Tin Alloyed Catalysts for the Ethanol Oxidation Reaction in an Alkaline Medium. *ACS Catal.* **2012**, *2* (2), 287−297.

(34) Kahyarian, A.; Brown, B.; Nesic, S. Mechanism of the Hydrogen Evolution Reaction in Mildly Acidic Environments on Gold. *J. Electrochem. Soc.* **2017**, *164* (6), H365−H374.

(35) Durst, J.; Simon, C.; Hasché, F.; Gasteiger, H. A. Hydrogen Oxidation and Evolution Reaction Kinetics on Carbon Supported Pt, Ir, Rh, and Pd Electrocatalysts in Acidic Media. *J. Electrochem. Soc.* **2015**, *162* (1), F190−F203.

(36) Gong, Q.; Cheng, L.; Liu, C.; Zhang, M.; Feng, Q.; Ye, H.; Zeng, M.; Xie, L.; Liu, Z.; Li, Y. Ultrathin $MoS_{2(1-x)}Se_{2x}$ Alloy Nanoflakes For Electrocatalytic Hydrogen Evolution Reaction. *ACS Catal.* **2015**, *5* (4), 2213−2219.

(37) Lado, J. L.; Wang, X.; Paz, E.; Carbó-Argibay, E.; Guldris, N.; Rodríguez-Abreu, C.; Liu, L.; Kovnir, K.; Kolen'ko, Y. V. Design and Synthesis of Highly Active Al-Ni-P Foam Electrode for Hydrogen Evolution Reaction. *ACS Catal.* **2015**, *5* (11), 6503−6508.

(38) Laursen, A. B.; Wexler, R. B.; Whitaker, M. J.; Izett, E. J.; Calvinho, K. U. D.; Hwang, S.; Rucker, R.; Wang, H.; Li, J.; Garfunkel, E.; Greenblatt, M.; Rappe, A. M.; Dismukes, G. C. Climbing the Volcano of Electrocatalytic Activity while Avoiding Catalyst Corrosion: Ni_3P, a Hydrogen Evolution Electrocatalyst Stable in Both Acid and Alkali. *ACS Catal.* **2018**, *8* (5), 4408−4419.

(39) Feng, W.; Pang, W.; Xu, Y.; Guo, A.; Gao, X.; Qiu, X.; Chen, W. Transition Metal Selenides for Electrocatalytic Hydrogen Evolution Reaction. *ChemElectroChem* **2020**, *7*, 31−54.